


# Finding the grain size distribution that produces the densest arrangement in frictional sphere packings: Revisiting and rediscovering the century-old Fuller and Thompson distribution

William Fernando Oquendo-Patiño <sup>\*</sup>

*Departamento de Física, Facultad de Ciencias, Universidad Nacional de Colombia, Bogotá 111321, Colombia*

Nicolas Estrada<sup>†</sup>

*Departamento de Ingeniería Civil y Ambiental, Facultad de Ingeniería, Universidad de los Andes, Bogotá 111711, Colombia*



(Received 1 February 2022; accepted 16 May 2022; published 6 June 2022)

By means of discrete-element methods, we investigate the joint effects of the grain size distribution (GSD) and contact friction on the structure of three-dimensional samples composed of spherical grains. Specifically, we compress these systems isotropically until jamming and then analyze their structure in terms of density, connectivity, coefficients of uniformity and curvature, and parameters of grading entropy. Our study focuses on power-law GSDs and particularly on the Fuller and Thompson distribution, proposed over a century ago. First, we show that, among the set of GSDs investigated, this particular distribution produces the densest and best-connected systems, falsifying a conjecture recently posed in the literature. Second, we find that the jamming packing fraction can be accurately predicted as a function of simple descriptors of the GSD, but among these descriptors the granular entropy concept proves to be the most useful. This allows for an alternative interpretation of both jamming and grading entropy concepts. Finally, we compare the Fuller and Thompson distribution with two well-known GSDs: that of the Apollonian sphere packing and that towards which granular systems evolve after intensive grain fracturing. Surprisingly, we find that these three GSDs are practically coincident in the limit of large size spans, despite having been introduced or discovered in different scientific contexts (i.e., engineering, mathematics, and earth sciences, respectively).

DOI: [10.1103/PhysRevE.105.064901](https://doi.org/10.1103/PhysRevE.105.064901)

## I. INTRODUCTION

Granular materials are composed of relatively large bodies that interact, producing emergent behaviors that touch the realms of gasses, liquids, and solids. The constituent bodies have different characteristics, such as size, shape, and strength. Both fundamentally and practically, it is interesting to understand how these bodies can be packed in such a way that their density is maximized. In fact, such packing problems date back to the early works of Kepler [1,2] and Gauss [3], but it is only recently that a definite general proof was presented by Hales for the special case of monodisperse spheres (i.e., with a single size) [4] and by other authors for polyhedral particles with simple symmetrical shapes [5,6].

For polydisperse systems (i.e., with different sizes), which are common in both natural and industrial contexts, it is difficult to find a general approach to obtain the densest packing. This is because density is affected by many variables, such as grain size distribution (GSD), friction among particles, particle shape, and building protocol. However, given the practical importance of maximizing density, one can find early engineering works that approached the problem. The most remarkable are probably the experimental works of Fuller, Thompson, and Talbot over a century ago [7–9]. A few years

later, these works were complemented by the systematic approaches by Furnas [10,11]. In particular, Fuller and Thomson found that GSDs with a certain shape produce the densest packings; these are the GSDs with a cumulative volume distribution (often referred to as the grading curve) described by

$$\rho(d) = \left( \frac{d - d_{\min}}{d_{\max} - d_{\min}} \right)^\eta, \quad (1)$$

with an exponent  $\eta \simeq 0.5$ ; here  $\rho$  is the mass percentage of particles with diameters smaller than  $d$ ,  $d_{\min}$  ( $d_{\max}$ ) is the minimum (maximum) diameter, and  $\lambda = d_{\max}/d_{\min}$  is the size span. The distribution of particle diameters  $N_p(d)$  is then given by

$$N_p(d) \propto \frac{d\rho/dd}{d^3} \propto \frac{(d - d_{\min})^{\eta-1}}{d^3}. \quad (2)$$

Ever since, these findings have been used as a design framework for proportioning concrete and pavements, almost without further systematic investigation.

Paradoxically, despite how old packing problems in polydisperse granular systems are and their practical importance, these problems have aroused little interest during recent decades. In particular, these problems have seldom been studied by means of a privileged analysis tool: simulations with discrete-element methods (DEMs). Among the first to exploit this research opportunity, we note the works of Voivret *et al.* [12], who studied the density, microstructure, and

<sup>\*</sup>wfoquendop@unal.edu.co

<sup>†</sup>n.estrada22@uniandes.edu.co




force transmission properties of two-dimensional (2D) systems composed of disks while varying both  $\lambda \in (1.5, 49)$  and the shape of the GSD through a cumulative  $\beta$  distribution. Similar studies were carried out for polygonal particles and  $\lambda \in (1, 19)$  [13,14], as well as for disks and elongated particles with  $\lambda \in (1.2, 39)$  [15,16]. In these works, the uniform distribution by volume, in which the volume of all size classes is the same, was identified as the one that maximizes the packing density. Other remarkable works can be found in Refs. [17–19], although exploring smaller values of  $\lambda$ . Also, some authors have studied the space filling properties of systems built by means of geometrical rules [20–24], including the special case of Apollonian packings [21,25,26].

More recently, the authors have used DEM to study the density, microstructure, and force transmission properties of 2D and 3D systems of frictionless particles while varying both  $\lambda \in (2, 32)$  and the shape of the GSD, which followed Eq. (1) [27–29]. A few more groups are also exploring the effects of the GSD in 3D systems. Some of these studies have been devoted to exploring the jamming transition in systems composed of spheres [30–32]. Others have focused on space filling properties, microstructure, and shear strength [33,34]. These works have used GSDs built through a cumulative  $\beta$  distribution, including the uniform distribution by volume, and the largest  $\lambda$  that have been explored are close to 9 and 5, respectively. Others have investigated polydisperse powders, finding good agreement between DEM simulations and experiments [35], and also the influence of some GSDs on the mechanical response of geopolymers in ceramics [36].

The previous review shows that the effects of the GSD are only starting to be explored in three dimensions, that the size span used in most DEM studies is rather small (i.e., 1.7 on average [27], while the typical  $\lambda$  in granular geomaterials can be close to 100 [37]), and that the effects of some important parameters (e.g., contact friction or grain shape) remain practically unexplored. The purpose of this work was to explore the effects of the GSD (i.e., both its size span and its shape) on the packing fraction and the microstructure of three-dimensional samples composed of spherical particles. We also explored the effects of contact friction, as a second parameter that affects the packing density and makes it possible to simulate more realistic packings.

To do this, we built and analyzed a set of  $280r$  different granular samples, where  $r \simeq 3$  is the number of repetitions, which were carried out in order to compute fluctuations. The GSD followed Eq. (1) and was thus characterized by two parameters: the size span  $\lambda$  and the shape  $\eta$ , which makes it possible to build almost monodisperse systems, the Fuller and Thompson distribution, and the uniform distribution by volume. These parameters were varied in the following ranges:  $\lambda \in \{2, 4, 8, 12, 16, 24, 32\}$  and  $\eta \in \{0.1, 0.2, \dots, 0.9, 1\}$ . In three dimensions, this broad range implied very large systems, with up to  $5 \times 10^5$  particles and, in some cases, more than  $10^6$  contacts. For each GSD, with a given set of parameters  $\lambda$  and  $\eta$ , contact friction was varied as  $\mu \in \{0, 0.2, 0.6, 0.8\}$ . Once generated, the systems were compressed quasistatically until reaching mechanical equilibrium. In this state, the samples were analyzed in terms of density, connectivity, coefficients of uniformity and curvature, and parameters of grading entropy.

The article is organized as follows. In Sec. II we present the GSD generation, sample construction, and isotropic compression procedures, followed by our results in Sec. III. We first explore the effects of both GSD and contact friction on usual micromechanical descriptors, such as solid fraction and connectivity. Second, we explore the relationship between the controlled variables and several quantitative descriptors of the GSD (i.e., coefficient of uniformity, coefficient of curvature, and parameters of grading entropy). In Sec. IV we compare our GSDs, and in particular that proposed by Fuller and Thompson, with other reference size distributions. In Sec. V we summarize our results and present some perspectives for future work.

In the following, the values of  $\lambda$ ,  $\eta$ , and  $\mu$  are color coded with the colormaps , , and , respectively. In general, solid lines will represent a theoretical or fit curve, while dotted or dashed lines are drawn as guides to the eye.

## II. METHODS

We used the soft-particle discrete-element method. Normal forces were calculated using the Hertz model, and tangential forces were modeled as springs including static friction [38,39]. The simulations were performed using the LIGGGHTS package [40] and distributed on multicore computers with the GNU parallel utility [41]. The Hertz model parameters used were a Young modulus of  $\simeq 5.0 \times 10^7$  Pa, a Poisson ratio of 0.45, a restitution coefficient of 0.1, and a time step of  $\simeq 10^{-6}$  s.<sup>1</sup> For the postprocessing stage, we only considered the particles that were at least one average radius away from the walls (similar results were obtained for distances of one and  $1\frac{1}{2}$  diameters). We used the library VORO++ [43] to precisely compute the void volume associated with each particle. By using this technique, we considered the irregular boundary of the subsystems considered in the analysis.

In the following sections we present further details on the two phases that composed our numerical experiment: generating samples with a given grain size distribution and densifying the samples by isotropic compression.

### A. Generation of the grain size distribution

For each sample, a set of diameters was generated following the GSD described by Eq. (1) and controlled by two parameters: the size span  $\lambda = d_{\max}/d_{\min}$  and the exponent  $\eta$ , which determined the shape of the grading curve. For instance,  $\eta = 0$  corresponds to a monodisperse system,  $\eta \simeq 0.5$  to the Fuller and Thompson distribution, and  $\eta = 1$  to the uniform distribution by volume. In order to control the quality of the samples, we binned (80 bins) the numerical samples generated by LIGGGHTS, which uses the algorithm described in Ref. [44]. On these samples, we computed the empirical grain size distribution (ESD) and compared it with the theoretical GSD. We only accepted samples if  $\max |ESD_i - GSD_i| < 0.05$ , where  $i$  is the bin number. To fulfill this criterion, the minimum number of particles varied greatly among

<sup>1</sup>More information about the Hertz model can be found in [42].

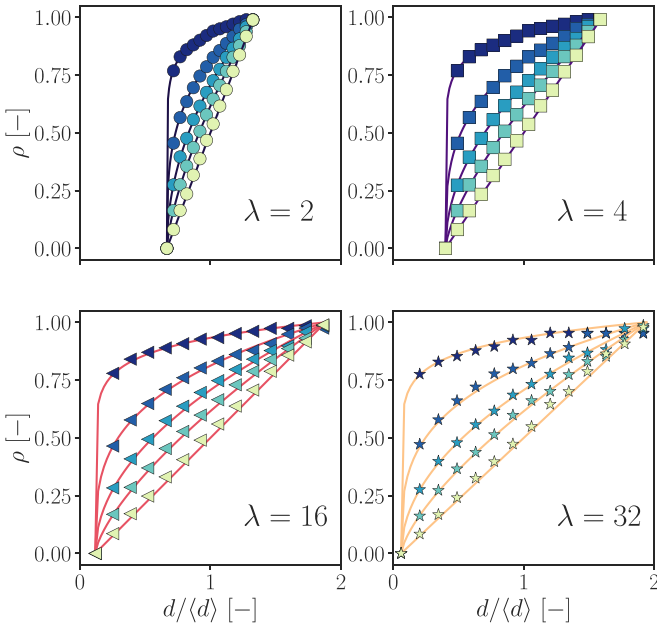


FIG. 1. Cumulative volume distributions (often referred to as grading curves), described by Eq. (1);  $\rho$  is the mass percentage of particles with diameters smaller than  $d$  and  $\langle d \rangle = (d_{\min} + d_{\max})/2$  is the average diameter. The data are for  $\eta = \{0.1, 0.3, 0.5, 0.7, 1\}$  and (a)  $\lambda = 2$ , (b)  $\lambda = 4$ , (c)  $\lambda = 16$ , and (d)  $\lambda = 32$ . The solid lines represent the theoretical GSD and the symbols correspond to the generated samples. Following the text convention, line colors and symbol shapes encode the parameter  $\lambda$ , while symbol colors encode  $\eta$ .

different combinations of  $\lambda$  and  $\eta$ . This representativity criterion is analogous to but somewhat simpler than the one used in Ref. [23]. Large  $\lambda$  and small  $\eta$  required systems with up to  $5 \times 10^5$  particles. The ratio of the minimum sample length  $L_{\min}$  to  $d_{50}$  (i.e., the diameter  $d$  for  $\rho = 0.5$ ) varied from around 20 for  $\lambda = 2$  to almost 120 for  $\lambda = 32$ . Figure 1 shows examples of the GSD for several values of  $\lambda$  and  $\eta$ .

### B. Isotropic compression

For each sample, once the GSD was generated, the particles were randomly distributed into a cubic box, with a small [i.e., close to 0.2 (0.01) for small (large)  $\lambda$ ] initial packing fraction

$$\phi = \frac{V_p}{V}, \quad (3)$$

where  $V_p$  is the volume occupied by the particles and  $V$  is the total volume. Then the diameter of the particles was slowly and uniformly increased until reaching a target value of  $\phi \simeq 0.4$  and the systems were left to relax. (It was verified that this target value did not influence the jamming packing fraction.)

Following this, the packings were isotropically compressed by applying a fixed force on all walls. The compression was slow (i.e., with an inertial number  $I \simeq 10^{-3}$  [45]) until reaching mechanical equilibrium (i.e., until jamming), which was quantified by means of two indicators: the normalized kinetic energy  $E$ , defined as the ratio of the total

kinetic energy over the total elastic potential energy, and the Cundall equilibrium parameter  $F$ , defined as the sum of the net force on all particles over the sum of the contact forces on all contacts. Simulations were stopped once  $E < 10^{-10}$  and  $F < 10^{-8}$ . For each GSD, we built systems with four different contact friction coefficients:  $\mu \in \{0, 0.2, 0.6, 0.8\}$ . Figure 2 illustrates the process of isotropic compression for a sample with  $\lambda = 12$ ,  $\eta = 0.5$ , and  $\mu = 0.2$  and Fig. 3 shows internal views of four systems with different values of  $\lambda$  and  $\eta$ , all four with  $\mu = 0.2$ .

As explained in Sec. I, each simulation was repeated around three times (i.e., from two to five times, due to computational constraints), using different initial positions. This is probably one of the simplest construction protocols that could be conceived, which is convenient for an initial investigation that could then be extended to study more realistic systems. In what follows, results are shown as the mean and the standard deviation. Both the generation of the GSD and the isotropic compression procedures are presented in more detail in Ref. [29].

## III. RESULTS

In the following sections we present the results of our study. We first present the effects of both GSD and contact friction on usual micromechanical descriptors, such as packing fraction and connectivity. Second, we present the relationship between the controlled variables and several quantitative descriptors of the GSD (i.e., coefficient of uniformity, coefficient of curvature, and parameters of grading entropy).

### A. Density

Density was quantified by means of the jamming packing fraction  $\phi_J$ . Figure 4 shows  $\phi_J$  as a function of the exponent  $\eta$ , for all values of the size span  $\lambda$  and for different values of the contact friction  $\mu$ . As explained in the following paragraphs, several key observations can be drawn from this set of figures.

On the one hand, we can see that  $\phi_J$  increases with  $\lambda$ , as is expected from intuition and from previous results. However, we can also see that, as  $\lambda$  increases, its effect on  $\phi_J$  decreases. As it will be shown later in this section, we find a dependence following a saturating exponential ansatz. In addition, we can observe that for large size spans (i.e., for  $\lambda \gtrsim 8$ ) there is a maximum value of  $\phi_J$ , for  $\eta$  between 0.4 and 0.6. It is remarkable that this range of  $\eta$  is very close to the optimal exponent found by Fuller and Thompson (i.e., 0.5). These effects are observed for all  $\mu$ , confirming that these are direct consequences of the GSD.

On the other hand, we can see that  $\phi_J$  decreases with  $\mu$ , showing that the systems become looser as the particles become more frictional. However, we can also see that the figures for  $\mu = 0.6$  and 0.8 are very similar, showing that the effects of  $\mu$  on  $\phi_J$  saturate for large contact friction. It is interesting to note that the jamming packing fraction observed in many of our systems exceeds that of the densest monodisperse sphere packings (i.e., 0.74 for the face-centered-cubic arrangement). Moreover, the maximum  $\phi_J$  observed in our samples (i.e., for  $\mu = 0$ , large  $\lambda$ , and  $\eta = 0.5$ )



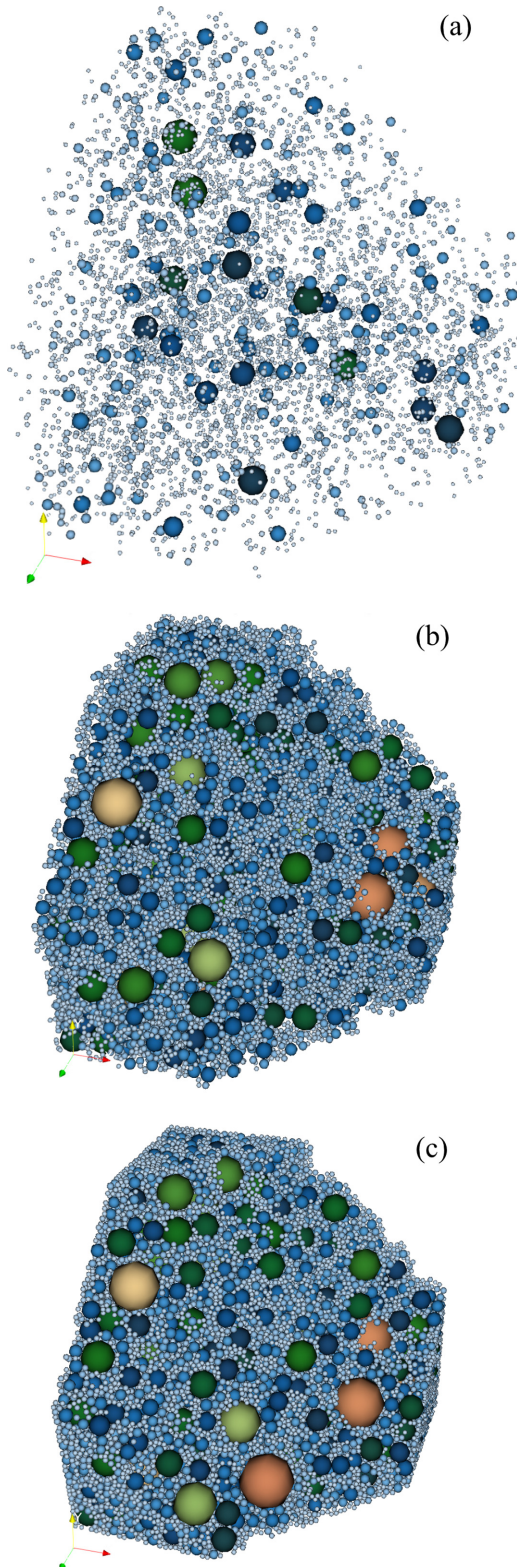


FIG. 2. Isotropic compression process for a system with a size span  $\lambda = 12$ , an exponent  $\eta = 0.5$ , and contact friction  $\mu = 0.2$  (a) after random placement of the particles in a square box, with a solid fraction  $\phi = 0.01$ , (b) after increasing the diameters and increasing  $\phi$  to 0.4, and (c) at the end of isotropic compression, after reaching mechanical equilibrium. Color encodes the particle radius.

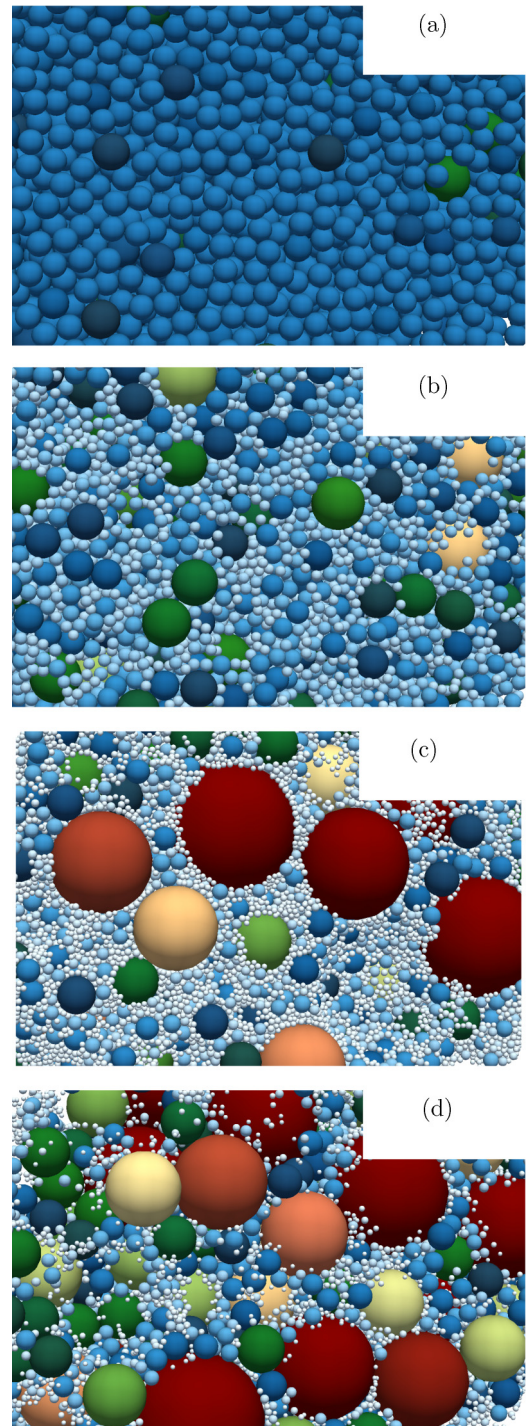


FIG. 3. Internal views for four systems after isotropic compression, with different values of the size span  $\lambda$  and the exponent  $\eta$  and for a contact friction  $\mu = 0.2$ : (a)  $\lambda = 2$  and  $\eta = 0.1$ , (b)  $\lambda = 8$  and  $\eta = 0.5$ , (c)  $\lambda = 32$  and  $\eta = 0.5$ , and (d)  $\lambda = 32$  and  $\eta = 1$ . Color encodes the particle radius.

is close to those found for monodisperse packings of Platonic (although below the density obtained with dodecahedra) and Archimedean (icosidodecahedron) solids [5]. Furthermore, for almost monodisperse systems ( $\lambda = 2$ , any  $\eta$ ) without

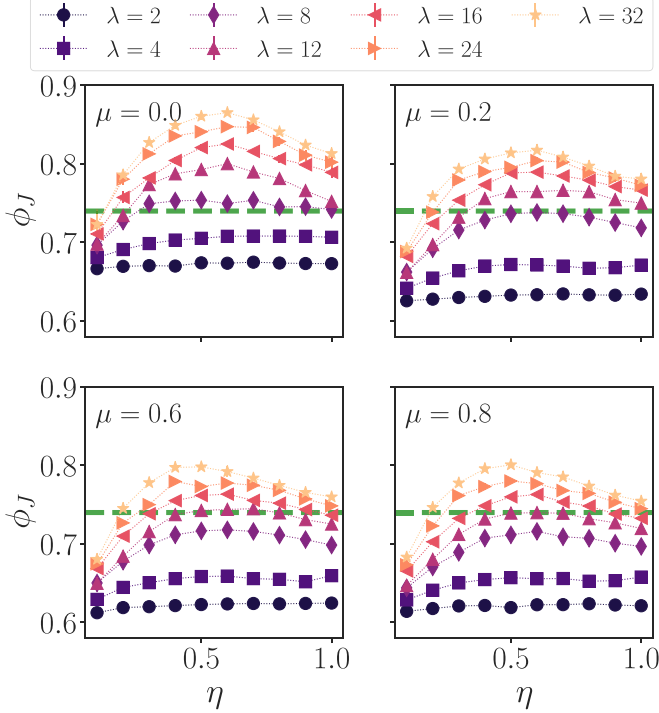


FIG. 4. Jamming packing fraction  $\phi_J$  as a function of the exponent  $\eta$ , for all values of the size span  $\lambda$  and for different values of the contact friction  $\mu$ : (a)  $\mu = 0.0$ , (b)  $\mu = 0.2$ , (c)  $\mu = 0.6$ , and (d)  $\mu = 0.8$ . Dashed lines show the maximal packing fraction for monodisperse systems (i.e., 0.74 for the face-centered-cubic arrangement). Error bars represent the standard deviation, although these are smaller than the symbols.

friction, we obtain a packing fraction around  $\simeq 0.67$  which is very close to the theoretical random close packing value  $\simeq 0.658963$ , recently predicted in [46] for exactly monodisperse frictionless systems.

In order to better analyze the relationship between  $\lambda$  and  $\phi_J$ , Fig. 5 shows  $\phi_J$  as a function of  $\lambda$ , for five different values of  $\eta$  and for two extreme values of  $\mu$ . First, we can see that the relationship between  $\lambda$  and  $\phi_J$  is not linear, in contrast to what has been found for small size spans [34]. Second, we observe that  $\phi_J$  for intermediate values of  $\eta$  generally exceed those found for  $\eta = 1$ . This implies that one can build systems for which  $\phi_J$  surpasses the limits of the triangular region posed in Ref. [34] as a conjecture. This region is shown as a gray triangle in Fig. 5.

We find that the relationship between  $\lambda$  and  $\phi_J$  is well described by a saturating exponential ansatz

$$\phi_J = \phi_{\min} + (\phi_{\max} - \phi_{\min})(1 - e^{-(\lambda-1)/\tau_\lambda}), \quad (4)$$

where  $\phi_{\min}$  ( $\phi_{\max}$ ) represents the minimal (maximal) jamming density and  $\tau_\lambda$  is the scale of the saturation to reach  $\phi_{\max}$ . We can put this relationship to the test by plotting  $(\phi_J - \phi_{\min})/(\phi_{\max} - \phi_{\min})$  as a function of  $(\lambda - 1)/\tau_\lambda$ . This is shown in Fig. 6, together with the evolution of  $\phi_{\min}$ ,  $\phi_{\max}$ , and  $\tau_\lambda$ . First, we can see that all data, for all  $\lambda$ ,  $\eta$ , and  $\mu$ , collapse under the universal curve described by Eq. (4). Second, we can also see that  $\phi_{\min}$  depends only on  $\mu$ . This is to be expected, since this is the jamming density for monodisperse systems.

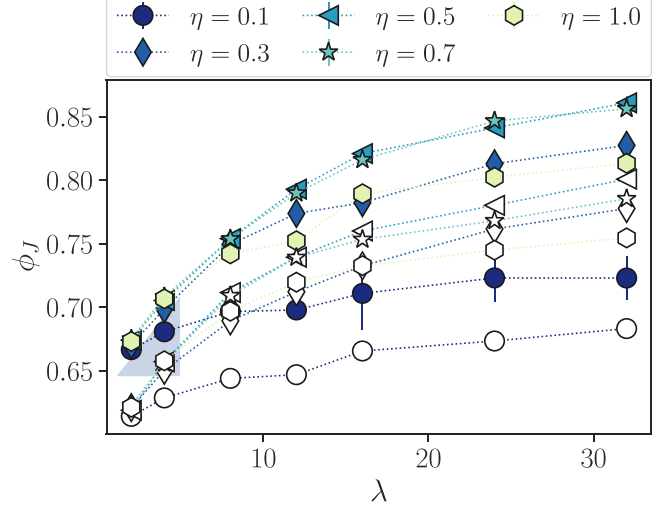


FIG. 5. Jamming packing fraction  $\phi_J$  as a function of the size span  $\lambda$ , for exponents  $\eta = \{0.1, 0.3, 0.5, 0.7, 1\}$  and for contact friction  $\mu = \{0, 0.8\}$ . Closed (open) symbols represent  $\mu = 0.0$  ( $0.8$ ). The highlighted triangular region corresponds to the accessible zone for  $\mu = 0$ , as conjectured in [34].

Third, we can observe that  $\phi_{\max}$  (i.e., the maximal jamming density that the system can reach in the limit of very large  $\lambda$ ) depends heavily on  $\eta$  and exhibits a maximum value for  $\eta \simeq 0.5$ , which again is coincident with the optimal exponent proposed by Fuller and Thompson. Finally, it is interesting to note that the scale  $\tau_\lambda$  seems to be independent of  $\eta$ .

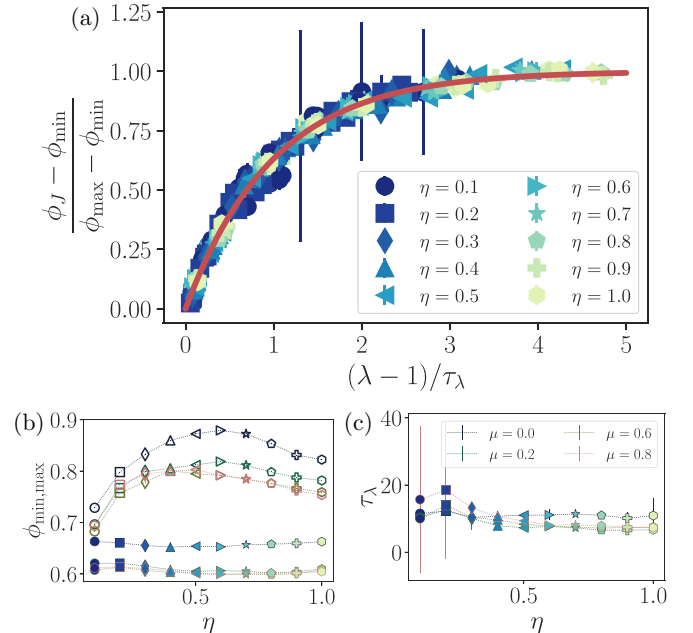


FIG. 6. (a) Normalized jamming packing fraction  $(\phi_J - \phi_{\min})/(\phi_{\max} - \phi_{\min})$  as a function of the scaled size span  $(\lambda - 1)/\tau_\lambda$ , for all values of the size span  $\lambda$ , the exponent  $\eta$ , and the contact friction  $\mu$ . The line shows the theoretical curve  $y = 1 - e^{-x}$ . (b) Minimal (closed symbols) and maximal (open symbols) jamming densities  $\phi_{\min}$  and  $\phi_{\max}$ , respectively, as functions of  $\eta$ , for all values of  $\mu$ , including error bars. (c) Scale  $\tau_\lambda$  as a function of  $\eta$ , for all values of  $\mu$ .



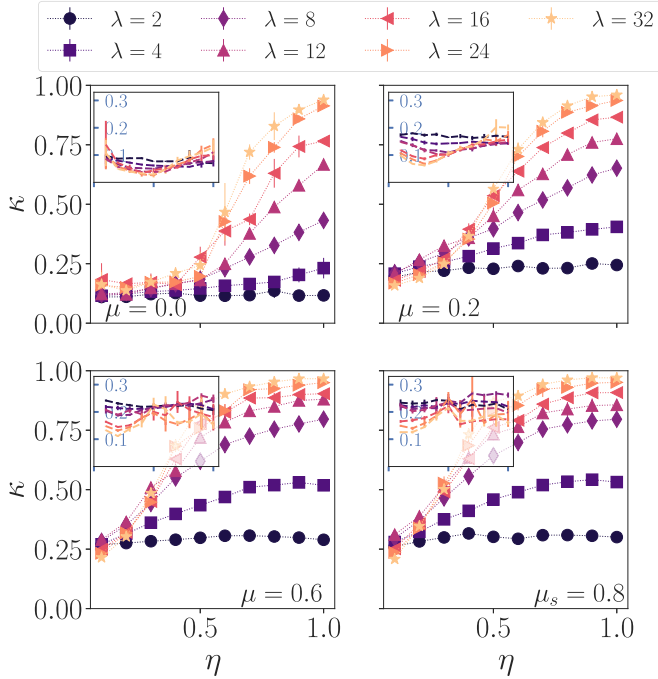


FIG. 7. Proportion of floating particles  $\kappa$  as a function of the exponent  $\eta$ , for all values of the size span  $\lambda$  and for different values of the contact friction  $\mu$ : (a)  $\mu = 0.0$ , (b)  $\mu = 0.2$ , (c)  $\mu = 0.6$ , and (d)  $\mu = 0.8$ . The insets show  $V_\kappa/V_p$ , the proportion of the particles' volume that is occupied by floating particles.

### B. Connectivity

The packings' connectivity was quantified by means of two indicators: the proportion of floating particles (rattlers)

$$\kappa = \frac{N_f}{N_p}, \quad (5)$$

where  $N_f$  is the proportion of particles with zero or one contact and  $N_p$  is the total number of particles, and the coordination number  $z$  (i.e., the mean number of contacts per particle)

$$z = \frac{2N_c}{N_p}, \quad (6)$$

where  $N_c$  is the total number of contacts. Figure 7 shows  $\kappa$  as a function of the exponent  $\eta$ , for all values of the size span  $\lambda$  and for different values of the contact friction  $\mu$ . First, we can see that  $\kappa$  increases with  $\lambda$ , reaching values as high as 95%, meaning that the force bearing network is composed of only 5% of the particles in the system. The insets show  $V_\kappa/V_p$ , the proportion of the particles' volume that is occupied by floating particles. We can see that, even if floating particles can be numerous, these particles are generally small and occupy a small volumetric fraction. The forces are thus being supported mainly by large particles. Second, we can see that  $\kappa$  heavily depends on  $\eta$ . Especially for low and intermediate values of  $\mu$  (i.e., 0 and 0.2),  $\kappa$  is low for  $\eta \leq 0.5$  and increases strongly for  $\eta \geq 0.5$ , reaching the highest values for the uniform distribution by volume (i.e., for  $\eta = 1$ ).

Figure 8 shows  $z$  as a function of  $\eta$ , for all values of  $\lambda$  and for different values of  $\mu$ . First, we can see that  $z$  reaches very

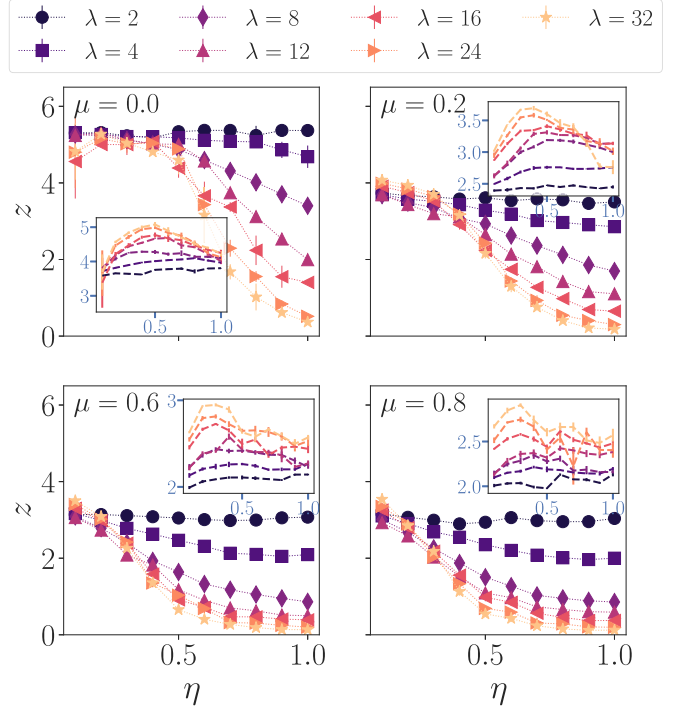


FIG. 8. Coordination number  $z$  as a function of the exponent  $\eta$ , for all values of the size span  $\lambda$  and for different values of the contact friction  $\mu$ : (a)  $\mu = 0.0$ , (b)  $\mu = 0.2$ , (c)  $\mu = 0.6$ , and (d)  $\mu = 0.8$ . The insets show  $z\phi_J(1 - V_\kappa/V_p)/(1 - \kappa)$ , which is proportional to the density of contacts and consequently to the systems' stiffness.

low values, which is a direct consequence of the high values of  $\kappa$  shown in Fig. 7. Second, we can see that  $z$  heavily depends on  $\eta$ . Again, especially for low and intermediate values of  $\mu$ ,  $z$  is high for  $\eta \leq 0.5$  and decreases drastically for  $\eta \geq 0.5$ , reaching the lowest values for the uniform distribution by volume. The insets show  $\phi_J z(1 - V_\kappa/V_p)/(1 - \kappa)$ , where  $\phi_J(1 - V_\kappa/V_p)$  is the solid fraction excluding the floating particles and  $z/(1 - \kappa)$  is the active coordination, which only takes into account the particles inside the force network. This quantity is important since it is proportional to the density of contacts and consequently to the system's stiffness [47]. Interestingly, the density of contacts is maximized when  $\eta$  is close to 0.5, with a slight translation to smaller values of  $\eta$  for larger  $\mu$ . These observations confirm that exponents that are close to those proposed by Fuller and Thompson produce systems that are not only very dense, but also very well connected.

### C. Quantitative descriptors of the grain size distribution

In this section we show that it is possible to compute key parameters from the GSD that allow us to predict which samples will be denser. These parameters are the uniformity and curvature coefficients, as well as the parameters of grading entropy.

#### 1. Coefficients of uniformity and curvature

Traditionally, civil engineers use two simple parameters to qualify the size span and shape of the GSD. The first is the

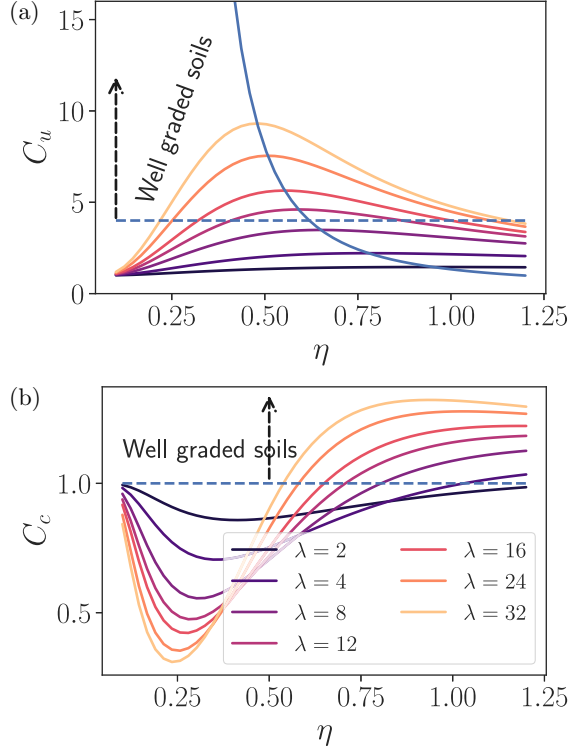


FIG. 9. Coefficients of (a) uniformity  $C_u$  and (b) curvature  $C_c$ , as functions of the exponent  $\eta$ , for all values of the size span  $\lambda$ . The dashed lines indicate the region of well-graded samples and the blue line connects the maximum values of  $C_u$ .

coefficient of uniformity  $C_u$ , defined as

$$C_u = \frac{d_{60}}{d_{10}}, \quad (7)$$

where  $d_{60}$  ( $d_{10}$ ) is the diameter for which  $\rho = 0.6$  (0.1) [see Eq. (1)]. As highlighted in Ref. [34], it is convenient to choose  $d_{60}$  ( $d_{10}$ ) as the representative size of large (small) particles, since  $d_{\min}$  and  $d_{\max}$  are not statistically relevant in volume or number. For the GSDs explored here,  $C_u$  can be computed exactly as

$$C_u = \frac{1 + 0.6^{1/\eta}(\lambda - 1)}{1 + 0.1^{1/\eta}(\lambda - 1)}, \quad (8)$$

and  $C_u \rightarrow 6^{1/\eta}$  for large size span  $\lambda$ . Usually, a sample is said to be well graded (i.e., with a sufficiently large size span) if  $C_u > 4$ . The second is the coefficient of curvature (sometimes called the coefficient of concavity)  $C_c$ , defined as

$$C_c = \frac{d_{30}^2}{d_{10}d_{60}}, \quad (9)$$

where  $d_{30}$  is the diameter for which  $\rho = 0.3$ . Like  $C_u$ ,  $C_c$  can be computed exactly as

$$C_c = \frac{[1 + 0.3^{1/\eta}(\lambda - 1)]^2}{[1 + 0.1^{1/\eta}(\lambda - 1)][1 + 0.6^{1/\eta}(\lambda - 1)]}, \quad (10)$$

and  $C_c \rightarrow (3/2)^{1/\eta}$  for large  $\lambda$ . A sample is considered well graded (i.e., with a grading curve with an “adequate” concavity) if  $1 < C_c < 3$ .

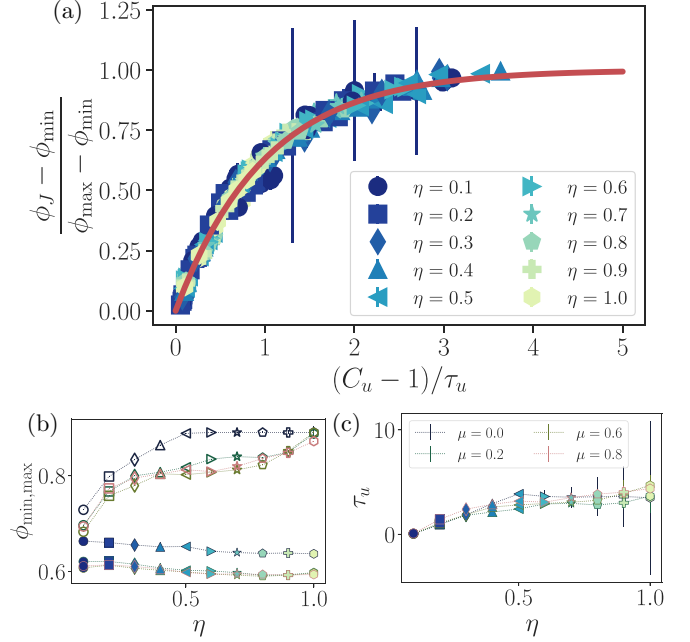


FIG. 10. (a) Normalized jamming packing fraction  $(\phi_J - \phi_{\min})/(\phi_{\max} - \phi_{\min})$  as a function of the scaled coefficient of uniformity  $(C_u - 1)/\tau_u$ , for all values of the size span  $\lambda$ , the exponent  $\eta$ , and the contact friction  $\mu$ . The line shows the theoretical curve  $y = 1 - e^{-x}$ . (b) Minimal (closed symbols) and maximal (open symbols) jamming densities  $\phi_{\min}$  and  $\phi_{\max}$ , respectively, as functions of  $\eta$ , for all values of  $\mu$ . (c) Scale  $\tau_u$  as a function of  $\eta$ , for all values of  $\mu$ .

Figure 9 shows  $C_u$  and  $C_c$  as functions of the exponent  $\eta$ , for all values of  $\lambda$ . The dashed lines indicate the region of well-graded samples and the blue line connects the maximum values of  $C_u$ . First, we can see that both  $C_u$  and  $C_c$  depend heavily on  $\lambda$  and  $\eta$ , with the most extreme values corresponding to large values of  $\lambda$ . Second, we can also see that, in order to have well-graded samples,  $\lambda$  must be larger than  $\sim 10$  and  $\eta$  must be intermediate or large. In fact, as shown by the blue line in Fig. 9(a), when  $\lambda$  is large  $C_u$  is maximized for values of  $\eta$  close to 0.5. Again, it is remarkable that this optimal value of the exponent is close to those proposed by Fuller and Thompson.

Recently, it was proposed that the jamming packing fraction  $\phi_J$  is proportional to  $C_u$  [34], although exploring relatively small size spans. We find that, as for  $\lambda$ , the relationship between  $C_u$  and  $\phi_J$  is well described by a saturating exponential ansatz:

$$\phi_J = \phi_{\min} + (\phi_{\max} - \phi_{\min})(1 - e^{-(C_u - 1)/\tau_u}). \quad (11)$$

Figure 10 shows  $(\phi_J - \phi_{\min})/(\phi_{\max} - \phi_{\min})$  as a function of  $(C_u - 1)/\tau_u$ , together with the evolution of  $\phi_{\min}$ ,  $\phi_{\max}$ , and  $\tau_u$ . As in Fig. 6, we can see that all data for all  $\lambda$ ,  $\eta$ , and  $\mu$  collapse under the universal curve described by Eq. (11). Therefore, both  $\lambda$  and  $C_u$  can be used to describe the packing density and their relationship is nonlinear. However, using any of these descriptors would require information on three parameters, i.e.,  $\phi_{\min}$ ,  $\phi_{\max}$ , and  $\tau_\lambda$  or  $\tau_u$ .

## 2. Grading entropy

Beyond practical parameters such as  $C_u$  and  $C_c$ , several researchers have explored the meaning and applicability of different theoretical ideas originated from the field of statistical physics. This is the case of the so-called grading entropy, initially formulated by Lőrincz [48,49] and then developed by Imre and co-workers [50–55].

Starting from the definition of statistical entropy for discrete systems, the grading entropy of a granular system is defined as

$$S = S_0 + \Delta S, \quad (12)$$

where  $S_0$  is called the base entropy and  $\Delta S$  is the entropy increment. In order to compute  $S$ , the GSD is divided into  $M$  fractions that subsequently double in size. These fractions are seen as the statistical cells of the distribution, and the representativity in each fraction is estimated through its mass proportion  $x_i$  with respect to the total mass. Then  $S_0$  and  $\Delta S$  can be calculated as

$$S_0 = \sum_{i=1}^M x_i \frac{\ln C_i}{\ln 2}, \quad (13)$$

$$\Delta S = -\frac{1}{\ln 2} \sum_{i=1}^M x_i \ln x_i,$$

where the sums run over all fractions  $M$  and  $C_i$  is the number of elementary cells comprising each fraction. The development of Eqs. (12) and (13) is presented in the Appendix. For further details, see Ref. [49].

Among both terms, it has been posed that only  $\Delta S$  plays the role of a “true” entropy in a thermodynamic sense [49]. This is reasonable, since  $\Delta S$  evokes an entropy of mixing between fractions (although it will be dependent on the actual discretization employed). It is thus interesting to explore the relationship between the jamming packing fraction  $\phi_J$  and  $\Delta S$ , the former being understood as the most probable macrostate in equilibrium and the latter as a measure of the number of microstates that would be compatible with that macrostate. The  $\Delta S$  could also be seen as a measure of the diversity of the GSD, as well as of the probability of particles filling void spaces. (Similar ideas are suggested in Ref. [56].)

Figure 11 shows  $\phi_J$  as a function of  $\Delta S$ , for all values of the size span  $\lambda$  and for different values of the contact friction  $\mu$ . We are excluding systems with an exponent  $\eta < 0.4$ , since it has been observed that these systems present some degree of local ordering [29]. Also, these systems are also related to ideal values for  $C_u$  and  $C_c$ . First, we can see that  $\phi_J$  increases with  $\Delta S$  in a nonlinear fashion. Second, as observed in Fig. 4, we can also see that  $\mu$  induces a vertical shift on  $\phi_J$ . Third, it is interesting to see that for each  $\mu$  all data collapse around the same trend, showing that  $\Delta S$  succeeds in capturing the effects of the GSD on  $\phi_J$ , in a more direct way than what can be achieved using simpler descriptors such as  $\lambda$  or  $C_u$ .

We find that the relationship between  $\Delta S$  and  $\phi_J$  is well described by a power-law ansatz

$$\phi_J = \phi_{\min} + C \Delta S^\alpha, \quad (14)$$

parametrized by the constant  $C$  and the exponent  $\alpha$ . We can put this relationship to the test by plotting  $(\phi_J - \phi_{\min})/C$  as

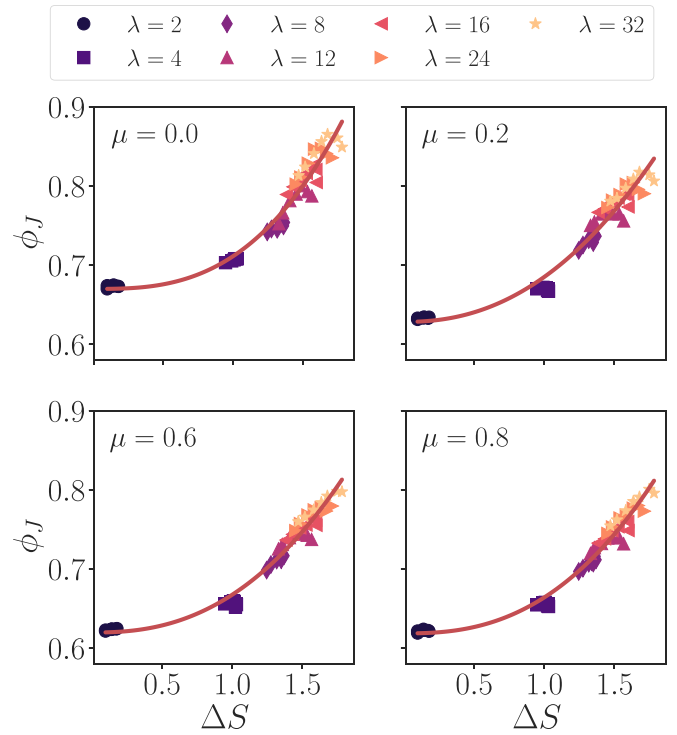


FIG. 11. Jamming packing fraction  $\phi_J$  as a function of the entropy increment  $\Delta S$ , for all values of the size span  $\lambda$ , for  $\eta \geq 0.4$ , and for different values of the contact friction  $\mu$ : (a)  $\mu = 0.0$ , (b)  $\mu = 0.2$ , (c)  $\mu = 0.6$ , and (d)  $\mu = 0.8$ .

a function of  $\Delta S^\alpha$ . This is shown in Fig. 12. We can see that all data for all  $\lambda$ ,  $\eta$ , and  $\mu$  collapse under the universal curve described by Eq. (14). This suggests that  $\Delta S$  can indeed be used to compare systems with different GSDs predicting which system will be denser, without actually performing any mechanical test; this, with two simple parameters  $C$  and  $\alpha$  that depend only on  $\mu$ , is shown in Table I.

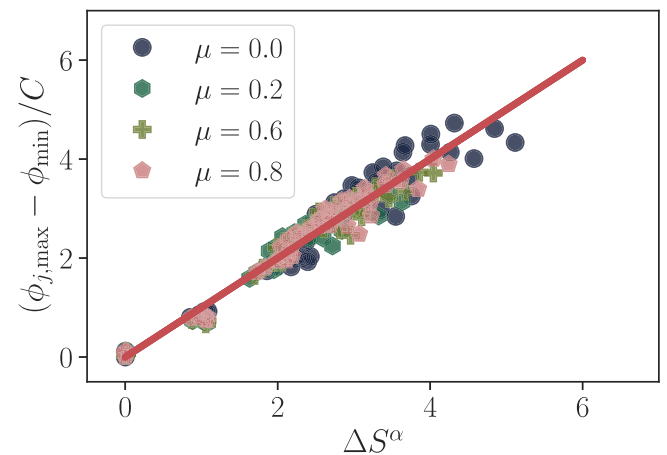


FIG. 12. Normalized jamming packing fraction  $\phi_{J,\max}$ , as a function of the entropy increment  $\Delta S$ , for all  $\lambda$ , for  $\eta \geq 0.4$ , and for different values of the contact friction  $\mu$ . The solid line is a guide to the eye and represents the line  $y = x$ . The fitting data are shown in Table I.



TABLE I. Fitting data for the universal curve describing Eq. (14) for all values of the contact friction  $\mu$ .

$\mu$	$\phi_{\min}$	$C$	$\alpha$
0.0	0.6699(1)	0.0413(2)	2.8(2)
0.2	0.6282(1)	0.0569(2)	2.2(4)
0.6	0.6197(1)	0.0478(1)	2.4(1)
0.8	0.6186(2)	0.0455(1)	2.5(1)

#### IV. COMPARISON WITH OTHER REFERENCE SIZE DISTRIBUTIONS

The previous sections were devoted to analyzing the grain size distributions described by Eq. (1) and among these that proposed by Fuller and Thompson (i.e., with an exponent  $\eta \simeq 0.5$ ) around a century ago. We showed that this GSD makes it possible to generate jammed granular systems with special properties, in terms of both density and microstructure. In this section we compare the Fuller and Thompson GSD with other reference GSDs.

On the one hand, let us consider the Apollonian sphere packing [57–59], based on the Apollonian gasket proposed by Leibniz in the 17th century and based on the works of Descartes and of course of Apollonius of Perga. This construction makes it possible to completely fill the space with mutually tangent spheres. The resulting set of spheres exhibits a fractal distribution with a fractal dimension  $D_f \simeq 2.473\,946\,5(1)$  [58], describing the asymptotic distribution

$$N_p(\epsilon) = \int_{\epsilon}^{\infty} N_p(d) dd \sim \epsilon^{-D_f}, \quad (15)$$

where  $N_p(\epsilon)$  is the number of spheres with a diameter  $d$  larger than the cutoff  $\epsilon$ . Considering Eq. (2), in the asymptotic case where  $d_{\min} \rightarrow 0$ , we have  $N_p(d) \propto d^{\eta-4}$  and  $N_p(\epsilon) \sim \epsilon^{\eta-3}$ . In this limit, the GSDs described by Eq. (1) are thus of fractal nature, with  $D_f = 3 - \eta$ . Interestingly, the exponent that corresponds to the Apollonian sphere packing is  $\eta = 3 - 2.473\,946\,5(1) \simeq 0.53$ , which is very close to the optimal value found by Fuller and Thompson.

On the other hand, let us consider the GSD towards which granular systems evolve after intensive grain fracturing. Tuccillo [60] showed that rocks that are subject to weathering, explosions, or impacts tend to break into a set of fragments that exhibits a fractal distribution, such as that described by Eq. (15) and with  $D_f \simeq 2.5$ . This leads to  $\eta \simeq 0.5$ . Sammis *et al.* [61] analyzed photographs of fault gouge, from faults that had accommodated large shear deformation and thus with intense levels of grain crushing. They found  $D_f \simeq 2.6$ , which corresponds to  $\eta \simeq 0.4$ . Close values of  $D_f$  in similar conditions have been found by other researchers, by means of both experiments [62,63] and numerical simulations [64,65]. Again, these exponents are remarkably close to those found by Fuller and Thompson.

#### V. CONCLUSION

The purpose of this article was to explore the joint effects of the grain size distribution and contact friction on

three-dimensional samples composed of spherical particles. To do so, we built and analyzed a large set of numerical samples with GSDs according to Eq. (1) (i.e., power-law GSDs) and thus described by two parameters, a size span and an exponent, which controlled the amplitude and the shape of the distribution, respectively. In order to satisfy statistical representativity, some samples needed to be very large, with almost  $5 \times 10^5$  particles and more than  $10^6$  contacts. These systems were compressed isotropically until reaching mechanical equilibrium (i.e., until jamming). In this state, the samples were analyzed in terms of density, connectivity, coefficients of uniformity and curvature, and parameters of grading entropy. The following paragraphs present our main findings and perspectives.

First, we found that intermediate values of the power-law exponent produce the densest packings for both frictionless and frictional systems. Furthermore, these exponents are close to the optimal exponent found by Fuller and Thompson a century ago. This agrees with previous findings for frictionless particles in two [27,28] and three dimensions [29]. At the same time, this differs from the results reported in Refs. [15,23,33,34], in which it was found that the GSD that produces the densest packing is the uniform distribution by volume; the origin of this disagreement is that these works only explored a subset of GSDs, which did not include the Fuller and Thompson distribution. In fact, we showed that introducing power-law GSDs with intermediate exponents (which can also be built by means of a cumulative  $\beta$  distribution) allows us to falsify the conjecture posed in Ref. [34], defining a region of accessible solid fractions as a function of the GSD.

Second, we found that using the Fuller and Thompson distribution allows for building packings that are not only very dense, but also very well connected. In fact, of the spectrum of GSDs explored, this particular distribution was the only one to simultaneously exhibit a low proportion of rattlers, a high coordination, and consequently a high density of contacts. This agrees with previous findings for frictionless particles in two [28] and three dimensions [29]. These general trends were shown to be independent of the contact friction, which in all cases played the role of decreasing the density and decreasing the connectivity of the system.

Third, we proposed a set of expressions that can be used to predict the jamming packing fraction as a function of quantitative descriptors of the GSD. These descriptors are the size span, the coefficient of uniformity, and the increment of grading entropy. Among these descriptors, the entropy increment allows a more direct prediction, with fewer parameters. This is to be expected, since both the size span and the coefficient of uniformity only include information on the amplitude of the distribution, whereas the entropy increment takes into account the amplitude and the shape of the GSD. Related ideas were presented in Refs. [34,51,56]. From a more theoretical perspective, we showed that it is interesting to explore the connections between the jammed state and its grading entropy, the former being understood as the most probable macrostate in equilibrium and the latter as a measure of the number of microstates that would be compatible with that macrostate. Grading entropy parameters can then be seen as a measure of the diversity of the GSD, as well as of the probability of particles filling void spaces, as suggested in Ref. [56].

Finally, we compared power-law GSDs, and in particular the Fuller and Thompson distribution, with two well-known GSDs: that of the Apollonian sphere packing and the GSD towards which granular systems evolve after intensive grain fracturing. Surprisingly, we found that these three GSDs are practically coincident in the limit of large size spans. We are unaware of other works that highlight this interesting connection between these distributions, identified in the engineering, mathematics, and earth sciences contexts. This suggests that the Fuller and Thompson distribution is indeed special, producing granular assemblies that are very dense, very well connected, and probably very resistant to grain crushing.

We believe that our findings are relevant for better understanding the effects of controlling the GSD on various properties of granular media. This knowledge is important, not only from a theoretical perspective, but also in numerous practical contexts that integrate the design of granular structures such as concrete and pavements. As initially shown by Fuller and Thompson, a smart proportioning of the granular phase in these composite materials can have enormous environmental and economic impacts. Our article also highlights the potential of discrete-element methods for exploring the effects of polydispersity, which remain poorly explored by the granular physics community.

Some interesting effects that were not approached in this article, but clearly merit further investigation, are (i) the effects of the GSD in the system's stiffness, as initially explored by Petit and Medina [66]; (ii) the effects of the GSD on shear strength, some of which are approached in Refs. [12, 14–16, 33]; and (iii) the verification of previous findings by means of experiments and more sophisticated simulations (e.g., with more realistic shapes and size spans).

#### ACKNOWLEDGMENTS

The authors acknowledge D. Barreto and E. Imre for introducing the topic of grading entropy and P. Mutabaruka for his help with  $\beta$ -function distributions. W.F.O.-P. acknowledges Universidad Nacional de Colombia for support through Projects No. 52655 and No. 55685; the RICAP HPC Latin-American network for partial support with HPC resources given through the fourth and sixth calls for projects provided by the CYTED cofunded Thematic Network RICAP (Grant No. 517RT0529); Powered@NLHPC, partially supported by the supercomputing infrastructure of the NLHPC (Grant No. ECM-02); and Nohora Cortes. N.E. thanks Catalina María Gutiérrez for helpful advice and stimulating discussions.

#### APPENDIX: PARAMETERS OF GRADING ENTROPY

In this Appendix we present further details on the development of the expressions used to calculate the grading entropy parameters introduced in Sec. III C 2. These ideas were borrowed from Ref. [49] and are rephrased here only for the purpose of completeness of the present article.

Consider a discrete system with  $N_e$  elements, distributed in  $M$  cells of equal size. The statistical entropy  $H$  of such a

system is given by

$$H = -N_e \sum_{i=1}^M \alpha_i \log_b \alpha_i, \quad (\text{A1})$$

where  $\alpha_i$  is the number proportion of the elements in the  $i$ th cell, with respect to  $N_e$ , and  $b$  is the base of the logarithm. If one sets to 1 the entropy of a system in equilibrium and with only two cells (i.e., for  $\alpha_1 = \alpha_2 = 0.5$ ), this leads to  $b = 2$ . The specific entropy  $S = H/N_e$  can then be rewritten as follows:

$$S = -\frac{1}{\ln 2} \sum_{i=1}^M \alpha_i \ln \alpha_i. \quad (\text{A2})$$

Consider now a polydisperse system, with elements of size  $d \in (d_{\min}, d_{\max})$ . Let us first define a minimal size of the statistical cells, which we will call fractions. The size of this elementary cell can be any size smaller than  $d_{\min}/2$ ; e.g., Lőrincz and co-workers often use the size of a SiO<sub>4</sub> tetrahedron:  $2^{-22}$  mm. Then let us prescribe that the size of subsequent fractions increases by a power of 2 (i.e., for any fraction  $i$ ,  $\Delta d_i = 2\Delta d_{i-1}$ , where  $\Delta d_i$  is the size of the fraction, given by the distance between its maximal and minimal diameters).

If it is assumed that the distribution of diameters inside the fractions is uniform, the number of elements inside the elementary cells is  $\alpha_i = x_i/C_i$ , where  $x_i$  is the mass proportion in the  $i$ th fraction, with respect to the total mass, and  $C_i$  is the number of elementary cells in the same fraction. The choice of a mass proportion instead of a number proportion may seem strange, but it is justified by the fact that most grading curves are determined from mass measures and not from grain counts. Moreover, the use of a number proportion is not necessarily correct, since the elements in different fractions are of different size and thus not directly interchangeable.

By substituting the new definition of  $\alpha_i$  into Eq. (A2), we obtain

$$\begin{aligned} S &= -\frac{1}{\ln 2} \sum_{i=1}^M \sum_{j=1}^{C_i} \alpha_j \ln \alpha_j \\ &= -\frac{1}{\ln 2} \sum_{i=1}^M x_i \ln \frac{x_i}{C_i} \\ &= \frac{1}{\ln 2} \sum_{i=1}^M x_i \ln C_i - \frac{1}{\ln 2} \sum_{i=1}^M x_i \ln x_i \\ &= S_0 + \Delta S. \end{aligned} \quad (\text{A3})$$

In this decomposition of  $S$ ,  $S_0$  is called the base entropy and  $\Delta S$  is called the entropy increment. From these expressions, it can be deduced that  $S_0$  is related to the skewness of the distribution (i.e., with the symmetry of  $x_i$  among fractions), while  $\Delta S$  is related to its peakedness. The precise physical meaning of  $S_0$  and  $\Delta S$  is yet to be determined. However, it has been posed that only  $\Delta S$  plays the role of a true entropy in a thermodynamic sense [49] (i.e., one that systematically increases when the system undergoes irreversible changes).

- [1] T. Aste and D. Weaire, *The Pursuit of Perfect Packing*, 2nd ed. (Taylor & Francis, London, 2008).
- [2] S. Torquato and F. H. Stillinger, *Rev. Mod. Phys.* **82**, 2633 (2010).
- [3] C. F. Gauß, *Göttingensche Gelehrte Anzeigen* **2**, 188 (1876).
- [4] T. Hales, *Ann. Math.* **162**, 1065 (2005).
- [5] S. Torquato and Y. Jiao, *Phys. Rev. E* **80**, 041104 (2009).
- [6] Y. Jiao, F. H. Stillinger, and S. Torquato, *Phys. Rev. Lett.* **100**, 245504 (2008).
- [7] W. B. Fuller and S. E. Thompson, *Trans. Am. Soc. Civ. Eng.* **59**, 67 (1907).
- [8] F. W. Taylor and S. E. Thompson, *A Treatise on Concrete, Plain and Reinforced* (Wiley, New York, 1905).
- [9] A. N. Talbot and F. E. Richart, *The Strength of Concrete, Its Relation to the Cement, Aggregates and Water* (University Of Illinois at Urbana Champaign, Urbana, 1923), Bulletin 137.
- [10] C. Furnas, The relations between specific volume, voids, and size composition in systems of broken solids of mixed sizes, Department of Commerce, Bureau of Mines Report No. 2894, 1929 (unpublished).
- [11] C. Furnas, *Ind. Eng. Chem.* **23**, 1052 (1931).
- [12] C. Voivret, F. Radjai, J.-Y. Delenne, and M. S. El Youssoufi, *Phys. Rev. Lett.* **102**, 178001 (2009).
- [13] D.-H. Nguyen, É. Azéma, F. Radjai, and P. Sornay, *Phys. Rev. E* **90**, 012202 (2014).
- [14] D.-H. Nguyen, E. Azéma, P. Sornay, and F. Radjai, *Phys. Rev. E* **91**, 032203 (2015).
- [15] E. Azéma, S. Linero, N. Estrada, and A. Lizcano, *EPJ. Web Conf.* **140**, 06001 (2017).
- [16] S. Linero Molina, E. Azema, N. Estrada, S. Fityus, J. Simmons, and A. Lizcano, *Geotech. Lett.* **9**, 328 (2019).
- [17] S. G. Bardenhagen, J. U. Brackbill, and D. L. Sulsky, *Phys. Rev. E* **62**, 3882 (2000).
- [18] M. Muthuswamy and A. Tordesillas, *J. Stat. Mech.* (2006) P09003.
- [19] M. R. Shaebani, M. Madadi, S. Luding, and D. E. Wolf, *Phys. Rev. E* **85**, 011301 (2012).
- [20] P. S. Dodds and J. S. Weitz, *Phys. Rev. E* **65**, 056108 (2002).
- [21] H. Herrmann, R. Mahmoodi Baram, and M. Wackenhut, *Physica A* **330**, 77 (2003).
- [22] K. Sobolev and A. Amirjanov, *Adv. Powder. Technol.* **15**, 365 (2004).
- [23] C. Voivret, F. Radjai, J.-Y. Delenne, and M. S. El Youssoufi, *Phys. Rev. E* **76**, 021301 (2007).
- [24] K. Sobolev and A. Amirjanov, *Constr. Build. Mater.* **24**, 1449 (2010).
- [25] T. Aste, *Phys. Rev. E* **53**, 2571 (1996).
- [26] S. D. Reis, N. A. Araújo, J. S. Andrade, Jr., and H. J. Herrmann, *Europhys Lett.* **97**, 18004 (2012).
- [27] N. Estrada, *Phys. Rev. E* **94**, 062903 (2016).
- [28] N. Estrada and W. F. Oquendo, *Phys. Rev. E* **96**, 042907 (2017).
- [29] W. F. Oquendo-Patiño and N. Estrada, *Granular Matter* **22**, 75 (2020).
- [30] V. Ogarko and S. Luding, *J. Chem. Phys.* **136**, 124508 (2012).
- [31] A. Santos, S. B. Yuste, M. López de Haro, G. Odriozola, and V. Ogarko, *Phys. Rev. E* **89**, 040302(R) (2014).
- [32] A. Santos, S. B. Yuste, M. López de Haro, and V. Ogarko, *Phys. Rev. E* **96**, 062603 (2017).
- [33] D. Cantor, E. Azéma, P. Sornay, and F. Radjai, *Phys. Rev. E* **98**, 052910 (2018).
- [34] P. Mutabaruka, M. Taiebat, R. J.-M. Pellenq, and F. Radjai, *Phys. Rev. E* **100**, 042906 (2019).
- [35] J. Schmidt, E. J. Parteli, N. Uhlmann, N. Wörlein, K.-E. Wirth, T. Pöschel, and W. Peukert, *Adv. Powder Technol.* **31**, 2293 (2020).
- [36] V. Pommer, E. Vejmelková, R. Černý, and M. Keppert, *Ceram. Int.* **47**, 31574 (2021).
- [37] A. Bolton, T. Brandon, J. Duncan, and J. Mitchell (unpublished).
- [38] T. Schwager and T. Pöschel, *Granular Matter* **9**, 465 (2007).
- [39] S. Luding, *Granular Matter* **10**, 235 (2008).
- [40] C. Kloss, C. Goniva, A. Hager, S. Amberger, and S. Pirker, *Prog. Comput. Fluid Dyn.* **12**, 140 (2012).
- [41] O. Tange, GNU Parallel 2018, available at <https://doi.org/10.5281/zenodo.1146014> (2018).
- [42] [https://www.cfdem.com/media/DEM/docu/gran\\_model\\_hertz.html](https://www.cfdem.com/media/DEM/docu/gran_model_hertz.html).
- [43] C. H. Rycroft, *Chaos* **19**, 041111 (2009).
- [44] E. Lozano, D. Roehl, W. Celes, and M. Gattass, *Comput. Math. Appl.* **71**, 1586 (2016).
- [45] GDR MiDi, *Eur. Phys. J. E* **14**, 341 (2004).
- [46] A. Zaccone, *Phys. Rev. Lett.* **128**, 028002 (2022).
- [47] M. H. Khalili, J.-N. Roux, J.-M. Pereira, S. Brisard, and M. Bornert, *Phys. Rev. E* **95**, 032908 (2017).
- [48] J. Lőrincz, Grading entropy of soils, Ph.D. thesis, Technical University of Budapest, 1986.
- [49] J. Lőrincz, E. Imre, M. Gálos, Q. P. Trang, K. Rajkai, S. Fityus, and G. Telekes, *Int. J. Geomech.* **5**, 311 (2005).
- [50] J. McDougall, E. Imre, D. Barreto, and D. Kelly, *Géotechnique* **63**, 262 (2013).
- [51] E. Imre, J. Lőrincz, Q. P. Trang, S. Fityus, J. Pusztai, G. Telekes, and T. Schanz, *Ksce. J. Civ. Eng.* **13**, 257 (2009).
- [52] E. Imre, J. Lőrincz, J. Szendefy, P. Q. Trang, L. Nagy, V. P. Singh, and S. Fityus, *Entropy* **14**, 1079 (2012).
- [53] J. Lőrincz, E. Imre, S. Fityus, P. Trang, T. Tarnai, I. Talata, and V. Singh, *Entropy* **17**, 2781 (2015).
- [54] J. Lőrincz, E. M. Imre, and V. P. Singh, in *Granular Materials*, edited by M. Sakellariou (InTech, London, 2017).
- [55] E. Imre and S. Fityus, *ce/papers* **2**, 639 (2018).
- [56] M. Á. Martín, M. Reyes, and F. J. Taguas, *Granular Matter* **19**, 9 (2017).
- [57] S. S. Manna and H. J. Herrmann, *J. Phys. A: Math. Gen.* **24**, L481 (1991).
- [58] M. Borkovec, W. D. Paris, and R. Peikert, *Fractals* **02**, 521 (1994).
- [59] S. V. Anishchik and N. N. Medvedev, *Phys. Rev. Lett.* **75**, 4314 (1995).
- [60] D. L. Turcotte, *J. Geophys. Res.* **91**, 1921 (1986).
- [61] C. Sammis, G. King, and R. Biegel, *Pure Appl. Geophys.* **125**, 777 (1987).
- [62] A. C. Palmer and T. J. O. Sanderson, *Proc. R. Soc. A* **433**, 469 (1991).
- [63] G. B. Crosta, P. Frattini, and N. Fusi, *J. Geophys. Res.* **112**, F01006 (2007).
- [64] J. P. de Bono and G. R. McDowell, *Comput. Geotech.* **78**, 11 (2016).
- [65] P. S. Iliev, F. K. Wittel, and H. J. Herrmann, *Phys. Rev. E* **99**, 012904 (2019).
- [66] J. C. Petit and E. Medina, *Phys. Rev. E* **98**, 022903 (2018).